

# SymFET: A Proposed Symmetric Graphene Tunneling Field Effect Transistor

Pei Zhao, Randall M. Feenstra, Gong Gu and Debdeep Jena

**Abstract**—In this work, an analytical model to calculate the channel potential and current-voltage characteristics in a Symmetric tunneling Field-Effect-Transistor (SymFET) is presented. The current in a SymFET flows by tunneling from an n-type graphene layer to a p-type graphene layer. A large current peak occurs when the Dirac points are aligned at a particular drain-to-source bias  $V_{DS}$ . Our model shows that the current of the SymFET is very weakly dependent on temperature. The resonant current peak is controlled by chemical doping and applied gate bias. The on/off ratio increases with graphene coherence length and doping. The symmetric resonant peak is a good candidate for high-speed analog applications, and can enable digital logic similar to the BiSFET. Our analytical model also offers the benefit of permitting simple analysis of features such as the full-width-at-half-maximum (FWHM) of the resonant peak and higher order harmonics of the nonlinear current. The SymFET takes advantage of the perfect symmetry of the bandstructure of 2D graphene, a feature that is not present in conventional semiconductors.

## I. INTRODUCTION

Graphene is an atomically thin two dimensional (2D) crystal [1]. Due to the high mobility of carriers in it, their linear dispersion and perfect 2D confinement, graphene is being considered as a channel material for future electronic devices. However, some challenges such as opening a finite bandgap for digital applications still remain.

A distinguishing feature of graphene is its symmetric electronic bandstructure. The valence band is a perfect mirror image of the conduction band about the Dirac point. Such symmetry carries over to gapped 2D crystals such as hexagonal Boron Nitride (h-BN), and less so to transition metal dichalcogenides (such as Molybdenum Disulfide,  $\text{MoS}_2$ ) [2]. This unique bandstructure *symmetry* has not been sufficiently exploited for active device applications till date.

Most studies of graphene based devices have focused on carrier transport in the 2D plane of the crystal. Recently, however, carrier transport *out of the plane*, i.e., vertical to the graphene sheet, has received increased attention. These studies of out-of-plane charge transport in 2D crystals have been motivated by the proposal of the bilayer pseudo-spin FET (BiSFET) in 2009 [3]. The BiSFET exploits the fact that two graphene layers can be placed in close proximity and if populated by electrons and holes, the strong Coulomb attraction between them can lead to exciton formation. Excitons are bosonic quasiparticles, and

can undergo condensation below a certain critical temperature. Since the Fermi degeneracy in graphene is tunable over a large energy window, the critical temperature for the excitonic condensate has been calculated to be higher than room temperature. The formation of the excitonic condensate is expected to lead to a macroscopic tunneling current between the layers. Similar behavior has been observed at low temperatures and at high magnetic fields in coupled AlGaAs/GaAs electron-hole bilayers [4],[5]. The BiSFET thus has the potential to realize many-body excitonic tunneling phenomena at room temperature. The power dissipation in computing using the functionality of BiSFET is predicted to be many orders lower than conventional CMOS switching.

Stacking of different 2D crystals leads to a novel class of heterostructures [6]. For example, stacking graphene with BN results in a smooth surface, since BN shares the same hexagonal lattice structure with graphene. The absence of out-of-plane covalent bonds implies that strain effects in similar lattice mismatched heterostructures based on  $\text{sp}^3$ -bonded 3D crystals are much reduced, or perhaps even eliminated. At low carrier concentration  $n \sim 10^{11} \text{ cm}^{-2}$ , the device exhibits mobilities of the order of  $100,000 \text{ cm}^2/\text{V}\cdot\text{s}$  at room temperature, which is much higher than for graphene on  $\text{SiO}_2$  or SiC [7]. Electron transport *out* of the plane of graphene has also started receiving attention in experiments. For example, a graphene/BN/graphene sandwich heterostructure was recently reported [8], and interlayer electron transport was measured. This stacked graphene/BN/graphene heterostructure showed a room temperature switching ratio of 50 and 10,000 for a similar graphene/ $\text{MoS}_2$ /graphene structure [8]. Another recent report [9] showed that electrons can be moved from 2D graphene into and out of Silicon to form a variable barrier-height device (the Barristor).

As charge transport out of the plane of graphene receives increasing attention, a pertinent question emerges upon careful analysis of the proposed BiSFET device. What is the expected behavior of a similar device structure consisting of a graphene-insulator-graphene (GIG) p-n junction heterostructure, but in the *absence* of the many-body excitonic condensate? Similar devices already exist in III-V resonant tunneling diodes, where single-particle tunneling itself leads to a number of interesting and useful quantum phenomena that persist at room temperature. Negative differential resistance is one such effect. Single-particle tunneling current transport has found enhanced attention recently in homojunction and heterojunction Tunneling Field-Effect Transistors (TFETs). It has been measured across various semiconductor heterostructures at room temperature, highlighting its robustness [10].

One major novel feature of graphene is the perfect symmetry of the bandstructure, which can lead to enhanced functionality.

P. Zhao and D. Jena are with the Department of Electrical Engineering, University of Notre Dame, Notre Dame, IN 46556 USA, djena@nd.edu.

R. M. Feenstra is with Dept. Physics, Carnegie Mellon University, Pittsburgh, PA 15213, USA.

G. Gu is with Dept. Electrical Engineering and Computer Science, University of Tennessee, Knoxville, TN 37996, USA.

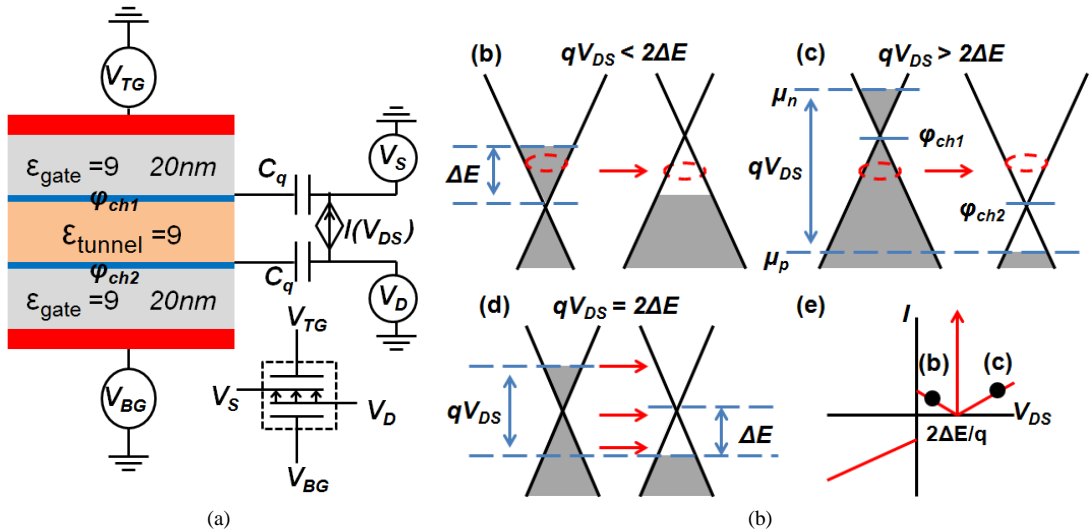


Fig. 1: (a) Sketch of the SymFET and the energy-band diagrams for a doped graphene/insulator/graphene junction, at voltages of (b)  $qV_{DS} < 2\Delta E$ , (c)  $qV_{DS} > 2\Delta E$ , and (d)  $qV_{DS} = 2\Delta E$ . A qualitative current-voltage  $I-V_{DS}$  characteristic is shown in (e). The inset in (a) shows the symbol defined for the SymFET.

Motivated by the above question, we recently calculated the single-particle interlayer tunneling current-voltage curves explicitly for finite area two-terminal GIG heterostructures [11]. The general finding was that at most interlayer bias voltages, energy and momentum conservations force a small tunneling current to flow at one particular energy halfway between the two Dirac points. However, at a particular interlayer voltage when the Dirac points of the p- and n-type graphene layers align, a very large interlayer tunneling current flows. This is because energy and momentum are conserved in this process for all electron energies between the quasi-Fermi levels of the n- and p-type graphene layers. The  $I-V$  curve is dominated by a Dirac-delta function-like peak at the critical interlayer voltage, and smaller currents at all other voltages. Our explicit calculation of the tunneling current also showed that the effect is highly robust to temperature, but less robust to rotational misalignment of the two graphene layers. This surprising, yet conceptually simple behavior of the 2-terminal GIG device leads naturally to the question: how will a transistor geometry with the single-particle GIG tunneling junction as its channel behave?

In this work, we extend the detailed physical model of the 2-terminal GIG device described in [11] to a *Symmetric* graphene tunneling *Field Effect Transistor*, which we call the ‘‘SymFET’’ since its unique characteristics derive from the symmetry of the bandstructure. We derive analytical expressions for the channel potential and current-voltage characteristics of the SymFET. Possible logic and high frequency applications are also discussed.

## II. DEVICE MODEL

We assume a symmetric device structure as shown in Fig. 1(a). Two graphene layers are separated by an insulator, and this GIG structure is sandwiched between a top and bottom gate. Ohmic contacts are formed to the two graphene layers individually representing the source (S) and the drain (D). The

top and bottom gate voltages  $V_{TG}, V_{BG}$  control the quasi-Fermi levels  $\mu_n$  and  $\mu_p$  in the top and bottom layers of graphene. The gate insulator thicknesses of both gates are assumed to be the same. The quasi-Fermi level is  $\Delta E$  above the Dirac point in the n-type graphene layer and below the Dirac point in the p-type graphene layer. This is indicated in Fig. 1(b), (c), and (d). The top and back gates are symmetric  $V_{TG} = -V_{BG}$ , and the drain-source voltage is  $V_{DS} = V_D - V_S$ . The inset in Fig. 1 (a) shows a proposed device symbol for the SymFET.

As shown in Fig. 1(b) and (c), under S/D biases when the two Dirac points are misaligned, only a single energy (and lateral k-momentum ring) in the Dirac cone meets the requirement of simultaneous energy and momentum conservation, and thus the tunneling current is small. At  $V_{DS} = 2\Delta E/q$ , however, the two Dirac points align, and electrons at *all* energies between the quasi-Fermi levels satisfy energy and momentum conservation. A large tunneling current is thus expected; a resonant current peak originating from the perfectly symmetric bandstructure of the graphene layers should result. Since graphene is not a metal, a part of the applied voltage will drop in the graphene layer itself. This effect of the finite density of states is captured in the quantum capacitance of graphene and is included in the model. This is critical since the gate capacitance  $C_g = \epsilon_g/t_g$  and the tunneling capacitance  $C_t = \epsilon_t/t_t$  are large and can reach the quantum capacitance limit easily [12]. For simplicity of the calculation we use the  $T \rightarrow 0K$  limit for quantum capacitance:

$$C_q = \frac{2}{\pi} \frac{|\Delta E|}{(\hbar v_F/q)^2}, \quad (1)$$

where  $q$  is the single electron charge,  $v_F$  is the Fermi velocity in graphene,  $\hbar$  is the reduced Planck constant. It can be verified that this approximation is a good one at room temperature.

The source and drain electrodes are assumed to be perfect ohmic contacts for simplicity. In practice, the contact resistance will also force a voltage drop, and can be added on top of

the intrinsic model. The interlayer tunneling current calculated in [11] depends on the interlayer voltage difference. Therefore, to find the behavior of the 4-terminal SymFET, potentials of the two graphene layers  $\varphi_{ch1}$  and  $\varphi_{ch2}$  need to be identified as a function of the gate and drain/source biases (the channel potentials of graphene and Fermi levels are referenced to the aligned channel potentials at flat band.). To do so, we invoke the charge neutrality condition:

$$\left(\frac{\varphi_{ch1}}{q} + V_{TG}\right)C_g + \left(\frac{\varphi_{ch1}}{q} - \frac{\varphi_{ch2}}{q}\right)C_t + \left(\frac{\varphi_{ch1}}{q} - \frac{\mu_n}{q}\right)C_q/2 + qN = 0, \quad (2)$$

$$\left(\frac{\varphi_{ch2}}{q} + V_{BG}\right)C_g + \left(\frac{\varphi_{ch2}}{q} - \frac{\varphi_{ch1}}{q}\right)C_t + \left(\frac{\varphi_{ch2}}{q} - \frac{\mu_p}{q}\right)C_q/2 - qN = 0, \quad (3)$$

where  $V_{TG} = -V_{BG} = V_G$ ,  $N = \Delta E_{doping}^2 / \pi(\hbar v_F)^2$  is the chemical doping concentration, and we assume the work functions of the metals are matched with the undoped graphene sheets which gives the flat-band conditions at zero gate bias. The factors 1/2 in the third terms of equations (2) and (3) are due to the linear dependence on  $\Delta E$  in the graphene quantum capacitance, which is a differential capacitance.

Then we take equation (2) minus equation (3), use relationships:  $qV_{DS} = 2\Delta E + \varphi_{ch1} - \varphi_{ch2}$ ,  $qV_{DS} = \mu_n - \mu_p$ ,  $\mu_n - \varphi_{ch1} = \Delta E$ , and  $\varphi_{ch2} - \mu_p = \Delta E$ , we can form a quadratic equation with the only unknown parameter  $\Delta E$ :

$$(V_{DS} - 2\frac{\Delta E}{q} + 2V_G)C_g + 2(V_{DS} - 2\frac{\Delta E}{q})C_t - \frac{2q\Delta E^2}{\pi(\hbar v_F)^2} + 2qN = 0, \quad (4)$$

and the solution is

$$\Delta E(V_G, V_{DS}) = -\frac{(2C_t + C_g)\pi(\hbar v_F/q)^2}{2} + \left\{ \frac{(2C_t + C_g)^2\pi^2(\hbar v_F/q)^4}{4} + \frac{\pi(\hbar v_F)^2}{2q} [(V_{DS} + 2V_G)C_g + 2C_tV_{DS} + 2qN] \right\}^{\frac{1}{2}}, \quad (5)$$

The electrostatic model used here is based on a 1D approximation, ignoring the intra-graphene layer potential distribution and current flows. A more rigorous treatment requires the solution of the 2D Poisson equation, which is suggested for future work.

The analytical expression for the interlayer tunneling current at zero temperature was derived in [11]. When the Dirac points in the two graphene layers are misaligned, the nonresonant tunneling current is:

$$I = G_1 \left( \frac{2\Delta E}{q} - V_{DS} \right), \quad (0 < qV_{DS} < 2\Delta E), \quad (6)$$

$$I = G_1 \left( V_{DS} - \frac{2\Delta E}{q} \right), \quad (qV_{DS} > 2\Delta E \text{ or } qV_{DS} < 0), \quad (7)$$

where the prefactor conductance  $G_1 = \frac{q^2 A}{2\hbar} \left( \frac{\hbar \kappa u_{12}^2 e^{-\kappa t}}{m d v_F} \right)^2$ ,  $\kappa$  is a decay constant for the tunneling current in barrier,  $m$  is the free

electron mass,  $d$  is the normalization constant for z-component wavefunction in graphene,  $u_{12}$  is a constant of order unity, and  $A = L^2$ , with  $L$  being the coherence length of graphene (size of ordered areas in graphene film). In this work, we assume the graphene size is  $A$  with coherence in all area.

The resonant current is a perfect Dirac-delta function at  $qV_{DS} = 2\Delta E$  for infinitely wide graphene sheets. For finite widths of length  $L$ , it is broadened to [11]:

$$I = \frac{1.6}{\sqrt{2\pi}} G_1 \frac{L\Delta E^2(2u_{11}^4 + u_{12}^4)}{u_{12}^4 q \hbar v_F} \exp\left[-\frac{A}{4\pi} \left(\frac{qV_{DS} - 2\Delta E}{\hbar v_F}\right)^2\right], \quad (8)$$

where  $u_{11}$  is a constant of order unity, similar to  $u_{12}$ . The total current is the combination of Equation (6) or Equation (7) summed up together with Equation (8).

Equations (6) - (8) were derived assuming zero temperature. At finite temperature, to capture the thermal occupation of states, the current needs to be calculated by including the Fermi-Dirac distributions in the integral over all states [11]. Equations (9) and (10) are the finite temperature expressions corresponding to Equations (6) and (7), derived by a direct extension of the theory in our previous work [11],

$$I = G_1 \frac{4\hbar^2 v_F^2}{q} \int_0^{+\infty} \left\{ k [f(E_{n,k} - \mu_n, T) - f(E_{p,k} - \mu_p, T)] \times \delta(2\Delta E - qV_{DS} - 2\hbar v_F k) \right\} dk \quad (9a)$$

$$= G_1 \left( \frac{2\Delta E}{q} - V_{DS} \right) [f(-qV_{DS}/2, T) - f(qV_{DS}/2, T)] \quad (9b)$$

$$= G_1 \left( \frac{2\Delta E}{q} - V_{DS} \right) \tanh\left(\frac{qV_{DS}}{4k_B T}\right), \quad (qV_{DS} < 2\Delta E) \quad (9c)$$

$$I = G_1 \frac{4\hbar^2 v_F^2}{q} \int_0^{+\infty} \left\{ k [f(E_{n,k} - \mu_n, T) - f(E_{p,k} - \mu_p, T)] \times \delta(qV_{DS} - 2\Delta E - 2\hbar v_F k) \right\} dk \quad (10a)$$

$$= G_1 \left( V_{DS} - \frac{2\Delta E}{q} \right) [f(-qV_{DS}/2, T) - f(qV_{DS}/2, T)] \quad (10b)$$

$$= G_1 \left( V_{DS} - \frac{2\Delta E}{q} \right) \tanh\left(\frac{qV_{DS}}{4k_B T}\right), \quad (qV_{DS} > 2\Delta E) \quad (10c)$$

where subscripts n and p refer to the n-type (top) and p-type (bottom) electrodes, respectively, and with the Fermi-Dirac distribution for arguments  $\delta E$  and T given by  $f(\delta E, T) \equiv 1/[1 + \exp(\delta E/k_B T)]$ . Following Ref. [11] we have for Eq. (9a), with  $0 < qV_{DS} < 2\Delta E$ , that  $E_{n,k} - \mu_n = \hbar v_F k - \Delta E$  and  $E_{p,k} - \mu_p = -\hbar v_F k + \Delta E$ , hence yielding Eqs. (9b) and (9c). Those equations also hold for  $qV_{DS} < 0$ , with the difference between the Fermi-Dirac occupation factors changing sign. For Eq. (10a), with  $qV_{DS} > 2\Delta E$ , we have  $E_{n,k} - \mu_n = -\hbar v_F k - \Delta E$  and  $E_{p,k} - \mu_p = \hbar v_F k + \Delta E$ , yielding Eqs.(10b) and (10c).

A finite-temperature correction to Eq. (8) is more complicated, since that equation itself is a significant approximation[11]. Nevertheless, the dominant term in its temperature dependence can be recognized as the increased number of states available for tunneling, in the resonant

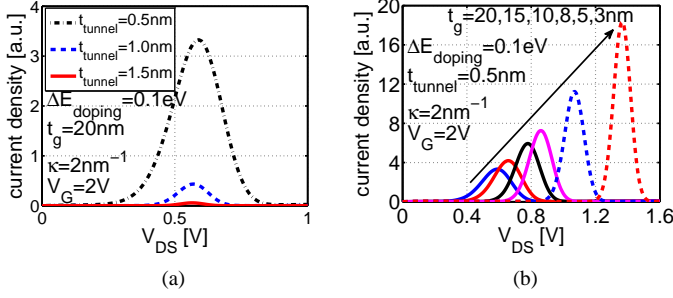


Fig. 2:  $I_D$  vs.  $V_{DS}$  characteristics showing scaling with (a) the tunneling insulator thickness and (b) the gate insulator thickness (an arbitrary  $\kappa$  value is chosen here to give a clear illustration of current density scaling).

situation of Fig. 1(d) with  $qV_{DS} = 2\Delta E$ . For this resonant situation the Dirac points of the two electrodes are aligned, at energy  $E_d$ . This number of states is given simply by

$$N_s(T) = \int_{-\infty}^{+\infty} \rho(E - E_d) [f(E - E_d - \Delta E, T) - f(E - E_d + \Delta E, T)] dE, \quad (11)$$

where  $\rho(E) = 2|E|/[\pi(\hbar v_F)^2]$  is the density-of-states (DOS) per unit area of graphene. Our correction to Eq. (8) is then made by multiplying it by  $N_s(T)/N_s(0)$ , with  $N_s(0) = 2\Delta E^2/[\pi(\hbar v_F)^2]$ . Expressing the result in terms of Fermi-Dirac integrals of order 1,  $\mathfrak{F}_1$ , we have

$$\frac{N_s(T)}{N_s(0)} = \frac{2(k_B T)^2}{\Delta E^2} [\mathfrak{F}_1(\frac{\Delta E}{k_B T}) - \mathfrak{F}_1(-\frac{\Delta E}{k_B T})] \quad (12)$$

where  $\mathfrak{F}_1(x) = \int_0^{+\infty} t/[1 + \exp(t - x)] dt$ .

Equations (9) and (10), as well as the product of Eqs. (8) and (12), are valid only in the limit of large  $L$ , although the  $L$  value at which the approximations break down is different for the two cases. In the former case, the dominant term in the slope of  $I(V_{DS})$  at  $V_{DS} = 0$  is  $qV_{DS}/4k_B T$ , arising from the tanh terms, and this slope becomes very large for small  $T$ . However, the exact solution for the current [11] yields a slope that is limited by the  $L$  value. We find that simply multiplying Eqs. (9) and (10) by a factor of  $\tanh(LqV_{DS}/\pi\hbar v_F)$  yields a slope at that agrees very well with the exact solution, and it does not significantly affect the  $I(V_{DS})$  curve elsewhere. For the product of Eqs. (8) and (12), the current from Eq. (8) is nonzero at  $V_{DS} = 0$ , with this discrepancy being significant only for sufficiently small  $L$  values. In this case we find that multiplying the product of Eqs. (8) and (12) by a factor of  $\tanh(LqV_{DS}/2\pi\hbar v_F)$  solves this problem of the nonzero current at  $V_{DS} = 0$ , and it also produces a slope at  $V_{DS} = 0$  that agrees fairly well with the exact solution. Hence, our final formula for the total current is given by

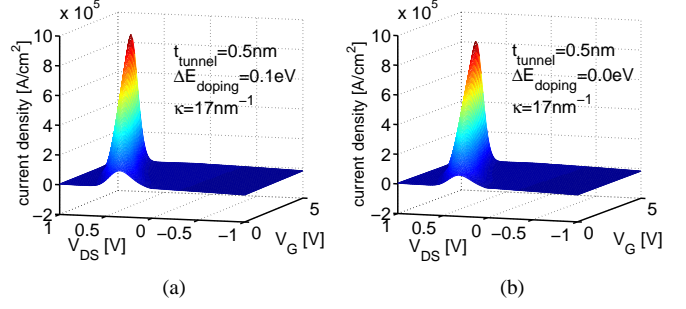


Fig. 3: The contour plot of the complete bias space for (a) chemical doping  $\Delta E_{doping} = 0.1 \text{ eV}$  and (b) no chemical doping.

$$I = G_1(V_{DS} - \frac{2\Delta E}{q}) \text{sgn}(V_{DS} - \frac{2\Delta E}{q}) \tanh(\frac{qV_{DS}}{4k_B T}) \tanh(\frac{LqV_{DS}}{\pi\hbar v_F}) + \left\{ \frac{1.6}{\sqrt{2\pi}} G_1 \frac{L\Delta E^2(2u_{11}^4 + u_{12}^4)}{u_{12}^4 q\hbar v_F} \exp[-\frac{A}{4\pi} (\frac{qV_{DS} - 2\Delta E}{\hbar v_F})^2] \right\} \times \frac{N_s(T)}{N_s(0)} \tanh(\frac{LqV_{DS}}{2\pi\hbar v_F}) \quad (13)$$

where  $\text{sgn}(V_{DS} - 2\Delta E/q)$  equals 1 for  $V_{DS} > 2\Delta E/q$ , 0 for  $V_{DS} = 2\Delta E/q$ , or -1 for  $V_{DS} < 2\Delta E/q$ .

The single particle tunneling model used in this work captures the relevant physics e.g. wave function overlap (detailed derivation in Ref. [11]), even in the case of strong inter-layer interactions at small insulator thicknesses. The only approximation we made is that the electronic structure (band structure) of the GIG system is the same as two non-interacting graphene sheets. We have justified the approximation as follows: any modification to the band structure due to the interaction will be near the Dirac energy. At sufficiently high doping  $\Delta E$ , the error is negligible.

### III. RESULTS AND DISCUSSIONS

We present typical  $I - V$  characteristics of the SymFET at room temperature first. The comparison of  $T = 300 \text{ K}$  and  $T = 0 \text{ K}$  is discussed later. The values of the decay constant  $\kappa$  can be calculated from the complex band structure inside the bandgap of the insulator based within the effective mass approximation [8]. Here, we use an estimated value  $\kappa = 17 \text{ nm}^{-1}$ , following footnote 14 of [11]. The chemical doping level is set to be  $\Delta E_{doping} = 0.1 \text{ eV}$ . A finite coherence length  $L = 100 \text{ nm}$  is assumed; the effect of this parameter on the on/off ratio for the device is discussed below. When the SymFET scales down to 50nm or less, momentum conservation does not scale well with device size. Scaling limits of SymFET will be a subject of future study; the quantum confinement and quantized transverse momentum in graphene nanoribbon also need to be considered near scaling limits, as discussed in Ref. [13].

The resultant  $I_D - V_{DS}$  characteristics with varying insulator thickness are shown in Fig. 2. The tunneling insulator thickness  $t_i$  is similar as the tunneling barrier thickness in double quantum well heterostructures [5]. As  $t_i$  increases the resonant

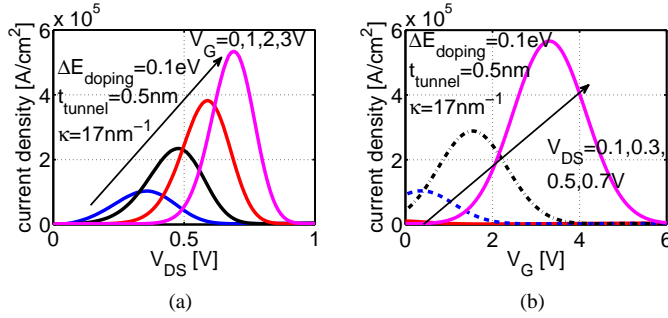


Fig. 4: (a)  $I_D$  vs.  $V_{DS}$  curves with different  $V_G$ , and (b)  $I_D$  vs.  $V_G$  at different  $V_{DS}$ .

peak current decreases, as expected. The gate insulator can be a high- $k$  material similar to that employed in Si CMOS technology. In addition, 2D materials such as BN might be a better choice to reduce the interface trap density since the dangling bond can be reduced. The measured breakdown field is as high as 7.94 MV/cm for BN [14]. Thinner  $t_g$  offers better gate control and higher gate induced doping. When  $t_g$  decreases,  $\Delta E$  becomes larger at same gate bias. The resonant peak moves to a higher bias and the peak current increases. For the simulation results shown next, we fix the gate capacitance with  $t_g = 20$  nm and dielectric contact  $\epsilon_g = 9$ , and the tunneling insulator thickness  $t_t = 0.5$  nm, and dielectric contact  $\epsilon_t = 9$ . (BN might have an even lower dielectric constant  $\epsilon_{BN} = 3.5$  [15]).

In Fig. 3, the entire bias phase space of the  $I-V$  characteristics are shown. When the graphene sheets are chemically doped (i.e.,  $\Delta E_{doping} = 0.1$  eV),  $V_{DS}$  drives the carriers tunneling between p- and n-type of graphene and the resonant peak exists for  $V_G = 0$  V. With non-zero  $V_G$ , gate electrostatic doping further increase  $\Delta E$  and resonant peak shift to higher  $V_{DS}$ . But the current is quite small in the non-resonant region.

If we define the peak current as the  $I_{on}$  and the current close to  $V_{DS} \sim 0$  as  $I_{off}$ , from Equation (6) and (8) the effective on/off ratio is:

$$\frac{I_{on}}{I_{off}} = \frac{0.8}{\sqrt{2\pi}} \frac{L\Delta E}{\hbar v_F}. \quad (14)$$

The effective on/off ratio is independent of temperature (ignoring the slight difference due to the Fermi tail), and increases with the doping  $\Delta E$  and the graphene size  $L$ . For  $L = 100$  nm the ratio is  $\sim 100$  and  $\sim 1000$  for  $L = 1$   $\mu\text{m}$ . We also point out that, the on/off ratio is not necessarily a figure of merit for the device (since the device might be employed for analog applications where high modulation is not required). In a similar vein, the resonant peak is symmetric in voltage, and represents a rather strong negative differential resistance. The peak-to-valley-current-ratio (PVCRR) of this NDR is identical to the on/off ratio defined above.

In Fig. 3 (b), we assume that  $\Delta E_{doping} = 0$  eV. At  $V_G = 0$  V,  $\Delta E$  is non-zero since drain bias also induces doping, similar as the case of GIG junction in [11]. However,  $\Delta E$  is small and the resonant peak is small at low  $V_G$ . When  $V_G$  increases, electrostatic doping induces an appreciable resonant current,

which further increases at higher  $V_G$ .

The  $I_D - V_{DS}$  characteristics at fixed  $V_G$  is shown in Fig. 4 (a). The resonant behavior shows clear on and off states without a saturation region. Because we assume a chemical doping of graphene, the SymFET with a resonant current peak can operate at  $V_G = 0$  V. As mentioned above, the gate will induce electrostatic doping in the graphene layer. With larger  $V_G$ ,  $\Delta E$  increases, the resonant condition  $qV_{DS} = 2\Delta E$  occurs at larger drain bias, and the resonant current peak moves to the right. Higher  $V_G$  induces more doping and thus large on-state current. In the 2-terminal GIG device, the resonant current peak is proportional to the coherence length  $L$ , and the width is proportional to  $1/L$  [11]. In the gated SymFET, since the gate bias electrostatically dopes the graphene, it offers the additional flexibility to adjust the on and off states. In Fig. 4 (b),  $I_D - V_G$  curves are shown with a strong non-linear and resonant behavior, but with wider peaks. When  $V_G$  is small and outside the resonant peak, the transconductance is small, but is large in the peak condition.

Different from the sub-threshold region of MOSFETs, we refer to the 'off' state away from the resonant peak in the SymFET as the non-resonant region. Although the graphene sheets are doped, according to conservation laws, the current near  $V_G = 0$  V is low ( $V_{DS} = 0.7$  V, solid line in Fig. 4 (b)). The gate voltage modulates the doping potential  $\Delta E$  in SymFET. By Eq. (5), at fixed  $V_{DS}$ , doping potential  $\Delta E$  is a sub-linear function of  $V_G$ . The current  $I_{DS}(V_G)$  at non-resonant region roughly follows the same hyperbolic form as the first term of  $I_{DS}(V_{DS})$  in Eq. (13):

$$I \propto \tanh\left(\frac{qV_G}{4k_B T}\right) \tanh\left(\frac{LqV_G}{\pi\hbar v_F}\right). \quad (15)$$

Hyperbolic functions may not offer a sharp subthreshold-swing (SS), but the SymFET is more attractive for analog applications, where the steep SS is not necessary.

The resonant current peak follows a normal distribution function  $I \sim \exp\left(-\frac{(qV_{DS}-\Delta E)^2}{2\sigma^2}\right)$ , with Full-width-at-half-maximum,  $FWHM = 2.3548\sigma$ , where  $\sigma = \frac{\sqrt{2\pi}\hbar v_F}{L}$  for the resonant peak in SymFET. In fact,  $\Delta E$  is not a constant but also dependent on  $V_{DS}$  and  $V_G$ , thus the FWHM shown here is only an approximation. The reason why a narrower FWHM occurs for  $V_{DS}$  compared with  $V_G$  in Fig. 4 relates with the large gate insulator thickness (weaker gate control). Smaller FWHM of  $V_G$  can be achieved with thinner gate insulator (not shown here).

Because tunneling is the main current transport mechanism, the  $I_D - V_{DS}$  curve is quite insensitive to temperature as shown in Fig. 5. But since the Fermi Dirac distribution smears out state occupancy at a finite temperature, slight differences can still be observed between  $T = 300$  K and  $T = 0$  K. At low  $V_{DS}$ , the transport energy window (between the quasi-Fermi levels  $\mu_n$  and  $\mu_p$ ) is small (Fig. 5 (b)). Then, the Fermi distribution smearing reduces the carrier density at higher temperature and the current decreases. The increase of the resonant peak current at room temperature is because the Fermi distribution tail extends to higher energy with more states. When the Dirac points are aligned, states at all energies conserve lateral



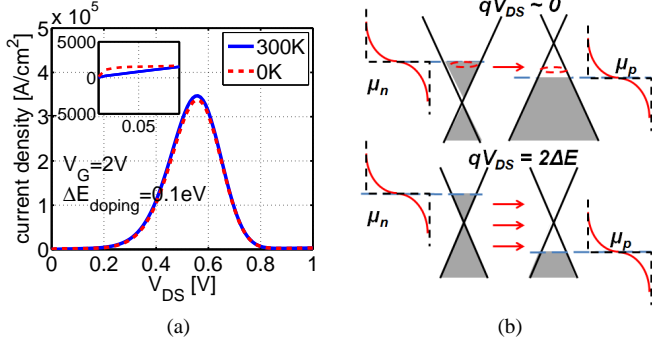


Fig. 5: (a) The comparison of  $I_D - V_{DS}$  characteristics at  $T = 300\text{K}$  and  $T = 0\text{K}$ . (b) the sketch of the band diagram and Fermi Dirac distribution at  $T = 300\text{K}$  and  $T = 0\text{K}$ . The inset of (a) shows the current density near  $V_{DS} = 0$

momentum upon tunneling, and thus are allowed.

We note that the device current has symmetric resonances in both the  $I_D - V_{DS}$  and  $I_D - V_G$  scans. This is quite unlike what happens in a single-layer graphene FET where the ‘ambipolar’ nature manifests itself primarily in the gate bias sweep [16] [17]. The nonlinear symmetric resonant  $I_D - V_{DS}$  behavior can be used for purpose of frequency multiplication (Fig. 6). If a DC voltage bias at the current peak  $V_{DS,p}$  is superimposed with an ac signal, the frequency of the output current will be doubled. We can use equation (8) to calculate the output ac current signal. Assuming that  $V_{DS} = V_{DS,p} + v_{ds}e^{i\omega t}$ , the oscillatory part of the current is:

$$I = \frac{1.6}{\sqrt{2\pi}} G_1 \frac{L\Delta E^2(2u_{11}^4 + u_{12}^4)}{u_{12}^4 q\hbar v_F} \exp\left(-\frac{A}{4\pi} \left[\frac{v_{ds}e^{i\omega t}}{\hbar v_F}\right]^2\right). \quad (16)$$

To find out the higher order harmonics, we ignore the constant prefactor:

$$I \propto \exp\left(-\frac{A}{4\pi} \left[\frac{v_{ds}e^{i\omega t}}{\hbar v_F}\right]^2\right). \quad (17)$$

This expression can be further extended as:

$$I \propto 1 - C_1 \exp(2j\omega t) + \frac{C_2^2}{2!} \exp(4j\omega t) - \frac{C_3^3}{3!} \exp(8j\omega t) + \dots, \quad (18)$$

where  $C_1 = \frac{A}{4\pi(\hbar v_F)^2} v_{ds}^2$ . In equation (18), only even higher harmonics occur.

The SymFET is expected to be intrinsically fast since it relies entirely on tunneling. The extrinsic performance with parasitics can be analyzed same as for any high speed device and will not be covered in this paper. High-frequency digital operation and a host of analog applications such as frequency multiplication are thus possible by exploiting the symmetry of the bandstructure of 2D graphene.

As explained in [11], the greatest amount of nonlinearity in the  $I - V$  characteristics is achieved with nearly perfect rotational orientation of graphene layers. This presents a significant challenge in fabrication of such devices based on the layer transfer technology. But epitaxial growth of

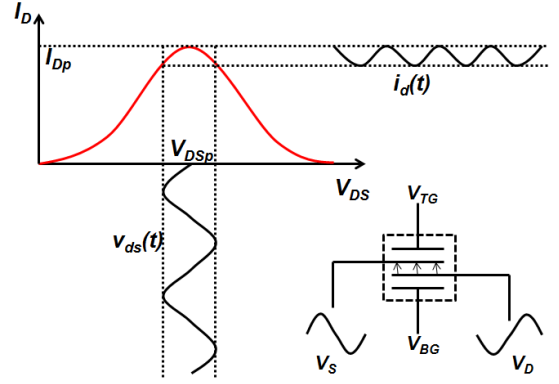


Fig. 6: The nonlinear resonant current is highly symmetric. When a DC voltage  $V_{DS,p}$  biased at the current peak is superimposed with an ac signal  $v_{ds}(t)$ , the frequency of the output current  $i(t)$  will be doubled.

graphene, BN [18] or other 2D materials provides a choice to overcome this problem. We note that due to the many-particle nature of the excitonic condensate, the BiSFET is expected to be insensitive to rotational misalignment [3]. This is similar to the robustness of superconductivity to defects. However, the single-particle tunneling nature also makes the SymFET robust to certain quantities to which the BiSFET is sensitive. As discussed earlier, the SymFET is robust to temperature. Another advantage is the robustness of single-particle tunneling - this is an intrinsic advantage for the SymFET. Although the tunneling current will vary with the tunneling insulator thickness and its dielectric constant, the regular single-particle tunneling behavior will survive in all temperature and thickness values. Thus, unlike the BiSFET’s sensitivity to thickness variations, the SymFET behavior is robust to thickness and dielectric constant variations. Both thickness variations and inelastic scattering processes can be significantly suppressed by using 2D crystal ‘insulators’ such as BN or MoS<sub>2</sub> between the graphene layers, preferably in a rotationally aligned structure.

In summary, we have presented an analytical model to calculate the channel doping potential and current-voltage characteristics in a novel electronic device structure, the SymFET. The current in a SymFET flows by tunneling from one graphene layer to the other. The current is insensitive to temperature. The resonant current peak is controlled by chemical doping and applied gate bias. The on/off ratio increases with graphene coherence length and doping. The symmetric resonant peak is a good candidate for high-speed analog applications, of which frequency multiplication is an example. The resonant peak behavior can also be the framework for new digital architectures that consume much lower power than the current state of the art electronic switches.

**Acknowledgements** This work was supported by the Semiconductor Research Corporation’s Nanoelectronics Research Initiative, the National Institute of Standards and Technology through the Midwest Institute for Nanoelectronics Discovery (MIND), and the National Science Foundation.

## REFERENCES

- [1] A. K. Geim and K. S. Novoselov, "The rise of graphene", *Nat. Mater.*, 6, 183, 2007.
- [2] A. H. Castro Neto and K. Novoselov, "Two-Dimensional Crystals: Beyond Graphene", *Materials Express*, 2158, 2011.
- [3] S. K. Banerjee, L. F. Register, E. Tutuc, D. Reddy, A. H. MacDonald, "Bilayer PseudoSpin Field-Effect Transistor (BiSFET): A Proposed New Logic Device", *IEEE Electron Device Lett.*, 30, 158, 2009.
- [4] J. P. Eisenstein, L. N. Pfeiffer, and K. W. West, "Field-induced resonant tunneling between parallel two-dimensional electron systems", *Appl. Phys. Lett.*, 58, 1497, 1991.
- [5] K. M. Brown, E. H. Linfield, D. A. Ritchie, G. A. C. Jones, M. P. Grinshaw, and M. Pepper, "Resonant tunneling between parallel, two-dimensional electron gases: A new approach to device fabrication using in situ ion beam lithography and molecular beam epitaxy growth", *Appl. Phys. Lett.*, 64, 1827, 1994.
- [6] C. R. Dean, A. F. Young, I. Meric, C. Lee, L. Wang, S. Sorgenfrei, K. Watanabe, T. Taniguchi, P. Kim, K. L. Shepard, and J. Home, "Boron nitride substrates for high-quality graphene electronics", *Nature Nanotech.*, 5, 722, 2010.
- [7] A. S. Mayorov et al, "Direct evidence for micron-scale ballistic transport in encapsulated graphene at room temperature", *Nano Lett.*, 11, 2396, 2011.
- [8] L. Britnell et al, "Field-effect tunneling transistor based on vertical graphene heterostructures", *Science*, 335, 947, 2012.
- [9] Heejun Yang et al, "Graphene Barristor, a Triode Device with a Gate-Controlled Schottky Barrier", *Science*, 336, 1140, 2012.
- [10] A. C. Seabaugh and Q. Zhang, "Low voltage tunnel transistors for beyond CMOS logic", *Proc. IEEE*, 98, 2095, 2010.
- [11] R. M. Feenstra, D. Jena, and G. Gu, "Single-Particle Tunneling in Doped Graphene-Insulator-Graphene Junctions", *J. Appl. Phys.*, 111, 043711, 2012.
- [12] S. Luryi, "Quantum capacitance devices", *Appl. Phys. Lett.*, 52, 501, 1988.
- [13] K. M. Masum Habib, Ferdows Zahid, and Roger K. Lake, "Negative differential resistance in bilayer graphene", *Appl. Phys. Lett.*, 98, 192112, 2011.
- [14] G.-H. Lee et al, "Electron tunneling through atomically flat and ultrathin hexagonal boron nitride", *Appl. Phys. Lett.*, 99, 243114, 2011.
- [15] C. R. Dean et al, "Multicomponent fractional quantum Hall effect in graphene", *Nature Physics*, 7, 693, 2011.
- [16] H. Wang, A. Hsu, K. K. Kim, J. Kong, and T. Palacios, "Gigahertz Ambipolar Frequency Multiplier based on CVD Graphene", *IEDM*, 572, 2010.
- [17] H. Wang, A. Hsu, J. Wu, J. Kong, and T. Palacios, "Graphene-Based Ambipolar RF Mixers", *Electron Dev. Lett.*, 31, 906, 2010.
- [18] A. Nagashima, N. Tejima, Y. Gamou, T. Kawai, and C. Oshima, "Electronic dispersion relations of monolayer hexagonal boron nitride formed on the Ni 111 surface", *Phys. Rev. B*, 51, 4606, 1995.